Penetration Mechanics Modeling & Validation of Blade Implements into Porous, Brittle Comet Simulant

Scott Jared Moreland,
Jet Propulsion Laboratory,
California Institute of Technology
4800 Oak Grove Dr.
Pasadena, CA 91109
scott.j.moreland@jpl.nasa.gov

Guillermo Fabian Diaz Lankenau,
Department of Mechanical Engineering,
Massachusetts Institute of Technology
77 Massachusetts Ave.,
Cambridge, MA 02139-4307
diazlank@mit.edu

Isabel Naranjo De Candido,
Scuola Superiore Sant'Anna,
Piazza Martiri della Libertà 33,
Pisa (Italy), 56127
isabeldecandido@gmail.com

Paul Backes,
Jet Propulsion Laboratory,
California Institute of Technology
4800 Oak Grove Dr.
Pasadena, CA 91109
Paul.g.backes@jpl.nasa.gov

Mircea Badescu,
Jet Propulsion Laboratory,
California Institute of Technology
4800 Oak Grove Dr.
Pasadena, CA 91109
mircea.badescu@jpl.nasa.gov

Abstract— **This paper presents an experimental and theoretical investigation of the interaction between a thin blade penetrator and materials representative of what is expected for the outermost 20cm of a comet's nucleus. The blade dimensions investigated are thicknesses of 1, 1.5mm and 2mm, width of 120 to 184mm, surface contact speeds of 0 to 15m/s, and penetration depth of up to 140mm. Earth snow is used as a conceptual comet analogue. Comet surface analogues used for experimentation are variations of foam glass and a simulant developed at the Jet Propulsion Laboratory.**

An apparatus developed for this study inserts blades into simulants via spring potential energy and blade kinetic energy. During insertion, recordings at >60kHz are made for forces acting on the blade and for the blade position. Parameters varied to explore effects on penetration dynamics include penetrated material, blade material and dimensions, blade speed at surface contact, and spring potential energy at blade surface contact.

The physics-based penetration model presented is shown to be useful for predicting the interaction between the blade shaped penetrators and comet-line materials. Behaviors predicted include penetration time, maximum penetration resistance, penetration velocity profile, and penetration resistance vs. depth profile. The model input variables are blade dimensions, comet microstructure strength, blade-comet friction (friction coefficient and cavity pressure), comet grain friction (as a damping coefficient), and system energy at contact.

The penetration model has applications beyond studying penetration behavior. An optimization routine is shown to be useful for estimating comet/simulant mechanical properties from experiments. The prediction of penetration performance for a large design space enables identification of advantageous designs with less experiments than would otherwise be practical.

TABLE OF CONTENTS

1. INTRODUCTION 1
2. MODEL DEVELOPMENT 2
3. EXPERIMENTAL APPARATUS 5
4. EXPERIMENTAL APPARATUS SOFTWARE 8
5. EXPERIMENTAL RESULTS AND VALIDATION 11
6. IMPORTANT FINDINGS RELATED TO DESIGN OF PENETRATORS 12
7. CONCLUSION 13
APPENDICES 14
A. VALIDATION TESTS GRILL BRICK 14
B. VALIDATION TESTS 2 OF 2, MPACS C 14
C. SENSITIVITY ANALYSIS FOR SIMULATED PENETRATION 16
ACKNOWLEDGEMENTS 17
REFERENCES 17
BIOGRAPHY 18

1. INTRODUCTION

This work herein develops and validates a penetration resistance model that represents the mechanics of thin blade interaction with porous, brittle materials representative of a comet surface. Further, software tools and methods of analysis were developed to aid in evaluating and improving a thin blade penetrator.

Past missions to comets have assayed the nucleus and helped increase our understanding of it. Of particular relevance to this paper are the NASA Deep Impact and ESA Rosetta missions. These two missions were the first to physically contact a comet nucleus. They have yielded a useful basis for

978-1-5090-1613-6/17/$31.00 ©2017 IEEE

estimating the mechanical strength of the outer layers of a comet nucleus.

The Deep Impact mission successfully orchestrated a collision between its own artificial impactor and comet Temple 1. The impactor weighed 370kgs and the relative speed at impact was approximately 10.2km/s. The impact yielded information about the nucleus' surface strength and structure despite observations being obstructed by an unexpectedly large dust cloud after impact [1].

The Rosetta mission succeeded in placing its lander, Philae, on the surface of comet 67P Churyumov–Gerasimenko. Due to a non-ideal final resting position, Philae has not been able to collect comet surface data to the full potential of its sensors. Surface small-scale strength estimates have still been calculated from Philae's bouncing on the comet's surface during landing [2].

Previous work on modelling comet penetration studied the mechanics of comet nucleus penetration using a cone-tipped penetrator [3]. The analytical and experimental results presented agree well with those described in this paper.

2. MODEL DEVELOPMENT

An analytical model for the penetration resistance of an implement inserted into comet-like materials enables more effective design of comet sampling devices (examples of devices in [4]). In this paper the penetrator will be a thin blade as seen in Figure 1 and described in section 3.

Penetration resistance is the net force acting on a penetrator body due to the interaction with a material during insertion. This net force is the sum of many contributions such as friction, material strength, material inertial resistance, etc.

Penetration into Earth's natural materials has been a field of interest for researchers for centuries. That body of research is leveraged for predicting comet penetration resistance. Most pertinent to this paper is penetration into snow-like materials with small, sub $5cm^2$ cross sectional area projectiles. Earth snow can be a reasonable analogue for comet nucleus surface material due to shared dominance of these attributes: high porosity, low density, brittleness, and cohesive bonding [1] [3] [5] [6].

Despite these similarities, colder-than-Earth temperatures on a comet's surface create significant differences in the mechanical properties of ice [5] [7]. A recommended adjustment to Earth models for more valid, conservative estimation of penetration resistance will be described in this section. A conservative estimation of comet penetration resistance is one likely to be above the actual value.

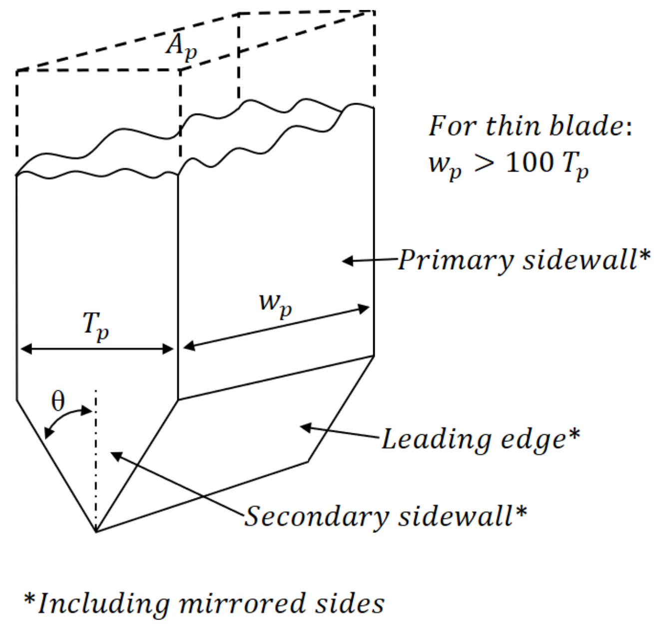

Figure 1. Labeled generic penetrator blade

Model Formulation for Penetration at Intermediate Speeds

The rate of penetration being considered in this paper occurs at speeds between 0m/s and 15m/s. This places it in a speed range uncommon for Earth snow penetration resistance models.

Modern applicable Earth snow penetration research is mostly separated into two categories, slow speed penetration occurring at less than 0.5m/s (snow structure characterization), and very high speed penetration occurring at more than 100 m/s (ballistics studies). The equations used to predict penetration resistance at those two speed ranges have important differences. At lower speeds it is assumed that penetration resistance is dominated by the structural strength of the material and friction between the penetrator tip and penetrated material [8]. At very high speeds penetration resistance is dominated by inertial forces from accelerating mass displaced during insertion [9].

It can be assumed that snow penetration at intermediate speeds would have to include the dominant forces from slow speed penetration and from very high speed penetration. This transition between dominant forms of penetration resistance as projectile speed decreases has been observed during terminal ballistics studies in Earth snow [9].

Slow Speed Penetration in Earth Snow

Previous work has shown that slow speed penetration into snow with penetrators of sub $5cm^2$ projected frontal area can be modelled as a function of penetrator shape and snow strength (Equation 1) [8] [10]. In these works, snow is assumed to be a solid foam-like material with a homogenous cellular structure, an idea well described in [11] and supported by the work of [12]. Experimental use of thin-blade penetrators is described in [13].

$$F_m = A_p S(\sin(\theta) + \mu\cos(\theta)), (\text{Eq. } 1)$$

F_m = Penetration Resistance for slow speed penetration
μ = coefficient of friction between penetrator blade leading edge and snow
A_p = Projected frontal area of penetrator ($T_p * w_p$)
θ = blade leading edge angle from vertical
S = microstructural strength of snow, see [8]

By utilizing a flat leading edge (i.e. θ = 90), Equation 1 is simplified to:

$$F_m = A_p S, (\text{Eq. } 2)$$

If the penetrated material has a cell size much smaller than the blade thickness and the penetrated material is known to not have internal fractures, the microstructural strength S can then be estimated directly from the experimental steady state penetration force.

Slow Speed Penetration in Comets Requires Depth Term

A term for sidewall friction force has been added to the model used in this paper. For Earth snow, friction force occurring at the blade sidewalls is usually negligible and thus ignored in common slow speed penetration models. Friction force is negligible due to small values for both the friction coefficient between the implement and snow, and the normal pressure exerted by the snow on the implement side walls. Friction coefficient and sidewall normal pressure may be significant in comets due to colder temperatures and presence of other hard materials.

Changes in friction coefficient: Snow generally does not generate a high friction surface at the moderately cold temperatures experienced in most locations humans inhabit. However, at extremely cold Earth temperatures snow's coefficient of friction rises abruptly [7]. A high coefficient of friction may also occur at comets since their surfaces temperatures are often below -70C [14].

Changes in sidewall pressure: Penetration into cellular solids – as is expected of porous cometary materials – is combination of deformation and fracturing of cells, as seen in Figure 2 and Figure 3. Fractured cell remnants are displaced and may occupy pores in the cellular solid. If the porosity is not sufficient to hold all dislodged grains, these grains exert pressure on the penetrator sidewalls and may create "bulb" ahead of the blade that can increase the blades apparent size.

During blade penetration in Earth snow the pressure the snow applies on the blade's sidewalls is usually negligible. This is because snow at Earth temperatures tends to deform plastically even for small deflections and because small penetrators will tend to push a snow "plug" ahead of them that is wider than the penetrator itself [9]. These two phenomenon combine to keep the cavity walls from exerting a significant normal force on the implement sidewalls. At the colder comet nucleus surface temperatures materials may be more rigidly coalesced and deform elastically, and the generation of a leading "plug" cannot be relied on to open a cavity larger than the blade cross section.

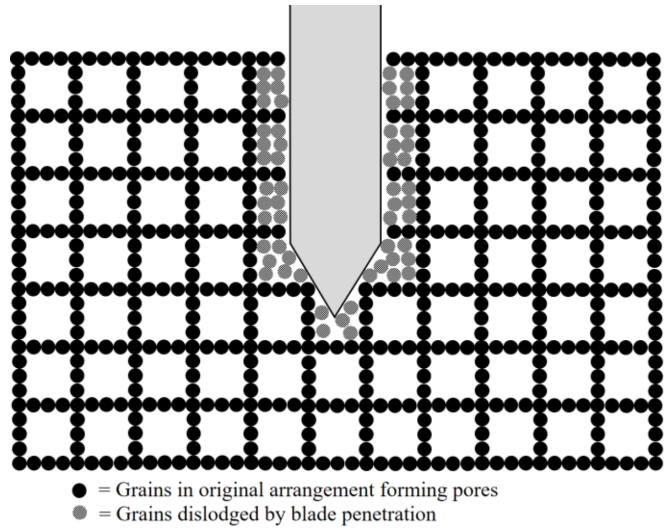

Figure 2. Penetration into idealized cellular solid with high porosity. As blade enters material it collapses grain structures around voids (pores). The proportion of solids (grains) to voids (pores) is such that dislodged grains can mostly occupy space that was formerly vacant. This results in low sidewall pressure on blade and in only a small volume of grains being affected during penetration.

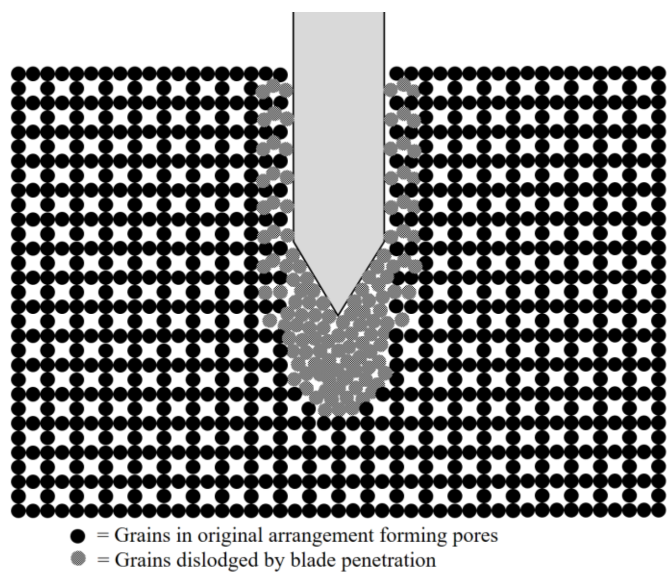

Figure 3. Penetration into idealized cellular solid lower porosity than Figure 2. As blade enters material it collapses grain structures around voids (pores). The proportion of solids (grains) to voids (pores) is such that dislodged grains find not enough open spaces to occupy and are pushed to dislodge other grains. This results in high sidewall pressures as the cellular structure pushes

the loose grains against blade. It may also result in a leading "plug" of disturbed material forming ahead of blade.

Penetration experiments performed for this paper replicate the expected comet friction conditions by using relatively soft 6061 aluminum blades to penetrate hard, well coalesced materials (Figure 4). These experiments showed penetration resistance to increase proportionally with the area of the penetrator parallel to penetration axis that has been inserted into the material. A potential explanation, if Coulomb friction is assumed, is that the penetrated material is exerting a constant sidewall pressure on the penetrator. An expression for sidewall friction would then be:

$$D_f = \mu P A_u(x), \text{(Eq. 3)}$$

For the constant cross section thin rectangular penetrators used in this study, primary sidewalls will be the dominant source of sidewall friction and secondary sidewall can be ignored. This is mostly because primary sidewalls are two orders of magnitude larger that secondary sidewalls and, to a lesser extent, because the angled leading face below primary sidewalls favors elastic deformation. Sidewall friction force can then be expressed as:

$$D_f = \mu P 2 w_p x, \text{(Eq. 4)}$$

In Equation 3 and Equation 4,
D_f = sidewall friction force
P = pressure on penetrator sidewalls exerted by material
μ = coefficient of friction
$A_u(x)$ = penetrator area underground parallel to penetration axis
w_p = rectangular penetrator width
x = penetration depth
Combining Equations 1 and 4, the expected slow speed penetration resistance of comets becomes:

$$P_s = A_p S(\sin(\theta) + \mu\cos(\theta)) + \mu P 2 w x, \text{(Eq. 5)}$$

Figure 4. Sliding penetrator blade on MPACS material creates smearing (MPACS, left) and scraping (6061 AL blade, right) parallel to direction of relative motion.

High Speed Penetration of Snow

The microstructural penetration resistance already described is still present in high speed penetration. However, forces that are a function of speed eventually become the dominant source of resistance at speeds above 100m/s.

There have been many penetration models developed for high speed, ballistics penetration. A useful differentiator between many of these models is whether they assume the penetrator to be rigid or deformable. In this paper it is assumed a penetrator could be engineered with the appropriate characteristics to be non-deformable as it penetrates into comet-like material.

A rigid penetrator greatly simplifies modelling because all the kinetic energy from the projectile is transferred to the penetrated medium and the penetrator geometry remains constant. The most basic and common models for a rigid penetrator moving through a natural medium are those that assume the penetration resistance force may be represented by a polynomial of the form shown in equation 6 [10]

$$D_H = C_0 + C_1\dot{x} + C_2\dot{x}^2, \text{(Eq. 6)}$$

Where,

D_H = high speed penetration resistance
C_n = coefficients
x = penetration depth

Snow penetration by ballistic projectiles suggests that when penetrating snow at speeds of about 100m/s or higher, the rightmost quadratic term in Equation 9 is dominant [11]. This term can be given a physical meaning as the inertia of displaced material of the penetrated medium (similar to aerodynamics and hydrodynamics). The suggested penetration resistance equation by [11] is,

$$D_I = K\,\rho\,A_p\,\dot{x}^2, \text{(Eq. 7)}$$

Where,
K = inertial (drag) coefficient for the projectile in snow
ρ = density of snow
A_p = approximated projected frontal area of blade
x = penetration depth

Damping Term Consideration

A damping term is added due to the penetration speed regimen being an intermediate point between speeds commonly studied. The damping term would correspond to the second term in Equation 6. Damping may occur during penetration from the friction between the grains that are flowing ahead of the blade as it cuts material. Additionally, as penetration speed increases there is less time to activate imperfections in the cellular (comet, snow) structure. This may affect penetration resistance and be perceived as damping.

The damping term depends on the penetration speed and the area of the blade projected along the penetration direction. It will be scaled by a damping constant. This may be defined as:

$$D = A_p C_1 \dot{x}, \text{ (Eq. 8)}$$

Where,
A_p = approximated projected frontal area of blade
C = Damping per unit area
x = penetration depth

Resulting Comet Surface Penetration Model

Combining all terms described in this section will yield a comet penetration model viable for penetrator blades of 1cm^2 to 5cm^2 cross section penetrating rigid foam-like materials at speeds up to15m/s. The resulting equation is:

$$R(x, \dot{x}) =$$

$$wT(S(\sin(\theta) + \mu\cos(\theta)) + \frac{\mu P\, 2\, x}{T} + C\dot{x} + K\rho\dot{x}^2), \text{ (Eq. 9)}$$

Where,
$R(x, \dot{x})$ = Penetration resistance
K = inertial coefficient for projectile in penetrated material
ρ = bulk density of penetrated material
w = width of rectangular blade
T = thickness of blade
S = microstructural strength
θ = blade leading edge angle
μ = friction coefficient
C = Coefficient of damping per unit area
x = penetration depth
P = pressure penetrated material exerts on blade sidewalls

Equation 9, describes the penetration resistance of a blade descending into a comet surface material. The form is intended to be coupled to a dynamic model (equations of motion) of the penetrator system to yield a complete continuous model. This approach is implemented in the following sections for a rectangular blade, spring energized penetrator at initial impact speeds of 0m/s to 15m/s into porous, brittle material.

3. EXPERIMENTAL APPARATUS

A specialized apparatus was developed to explore penetration into comet-analogue materials for sizes and dynamic conditions relevant to potential robotic sampling missions (Figure 5). The apparatus consisted of an instrumented, spring loaded blade penetrator system with easily-adjustable parameters and analysis software that initiates experiments, stores data, determines the penetration model coefficients described in Section 2, and graphically displays results intended for detailed analysis.

Physical Apparatus

The Blade Penetration Mechanics Apparatus utilizes sheet metal blades of primarily rectangular shape bent at the vertical centerline to 60° (Figure 7). Calculations in Section 2 utilize a rigid flat blade, however, for these experiments blades have been bent to make the thin metal construction stiffer. This simplification for calculations is valid under these assumptions:

- The penetrated material mechanical properties do not vary radially from the penetration axis (but they may vary with depth).
- The penetrated material is large enough in every direction to avoid changes in boundary conditions (cracking from boundaries verified not to exist via 5000fps camera)
- The penetrated surface is flat and normal to the penetration axis.
- The penetration blade is rigid.
- Penetration direction is a straight line parallel to the bend axis and normal to the flat face that will be penetrated. The penetrated material remains static for the experiments presented in this paper.
- The bend radius is large enough relative to penetrated-material grain size such that grains can flow into freely past the inside face of the bend radius.
- The opposing inside walls of the bent blade are far enough from each other such that the boundary conditions experienced by each blade face are equivalent for the bent and unbent cases.

The blade is mounted directly to a force-torque sensor to log penetration resistance. Note that the blade and blade mount have a small mass but accelerations are large. As the mass is between the penetrated resistance forces applied to the blade and the force-torque sensor, blade and blade mount inertial forces are unavoidably superposed over the penetration resistance. The apparatus software filters out blade and blade mount inertial forces via known mass and measured acceleration. This method provides closer-to-isolated measurement of the blade penetration resistance.

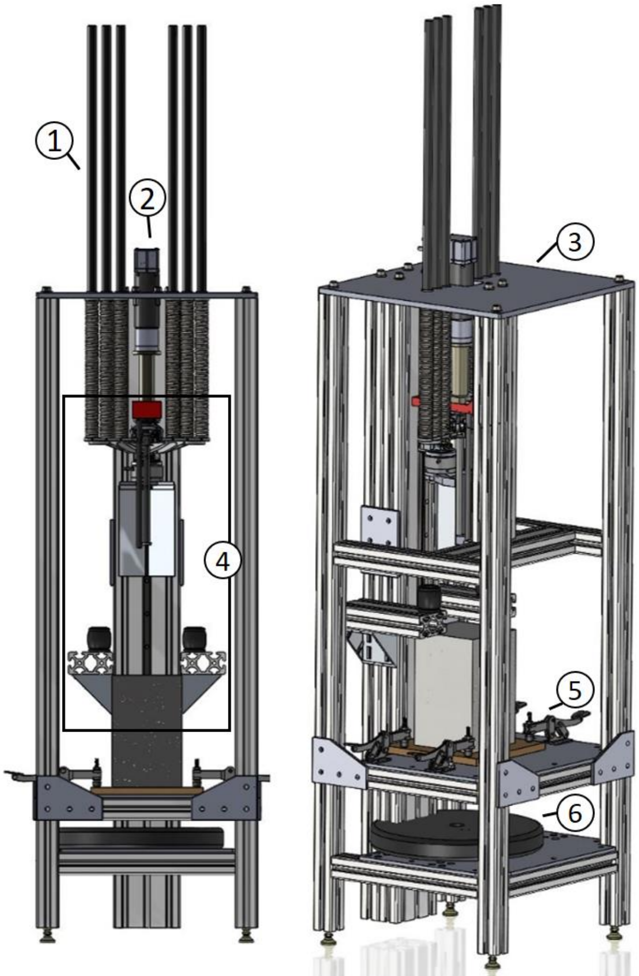

Figure 5. Blade penetration mechanics apparatus overview. Shown with springs compressed and ready to fire. The main structure constructed of aluminum extrusion is about 100cm tall and 35cm wide at its square base. (1) Cylindrical guides and holders for springs. (2) Actuator with encoder. Is connected to a roller-screw that compresses springs and triggers blade launch. (3) Plate to align spring guides, also holds string encoder base. (4) System close-up shown in Figure 6. (5) Lever locks to hold comet simulant in place. (6) Weight plate to improve stability.

The springs, force-torque sensor, ball bearing carriage (for guidance), firing mechanism locking feature, and string position sensors (incremental and absolute) all attach to a central mounting component that defines the accelerated body (Figure 6). The accelerated body and springs are retracted via a motor driven roller screw, compressing the springs, thus energizing the system. A hook latching system releases to fire the blade and accelerated body when commanded. Elastomer damping, high energy stops safely arrest motion at the end of travel if penetrator energy remains.

The main characteristics of the Blade Penetration Mechanics Apparatus are:

- Activation energy level settings of 92J, 184J, or 276J respectively by use of 2, 4 or 6 parallel springs.
- Variable initial stand-off position between zero stand-off and 30cm stand-off.
- Variable accelerated mass (primarily used to control blade initial impact velocity)
- Measurement of velocity/position/acceleration profile at high speed and high accuracy - 250KHz and 0.16mm resolution (high-speed impact string optical incremental encoder)
- Absolute position sensing and surface homing
- 500kHz 6 D.O.F. force/torque sensor at blade mount to measure penetration resistance
- Capable of applying 12MPa blade pressure statically, 35+MPa dynamically.
- Quick change clamp fixture to mount blade test specimens
- Securely fixture off-the-shelf or custom materials as comet surface analogues for testing
- All data streams typically recorded at 30kHz

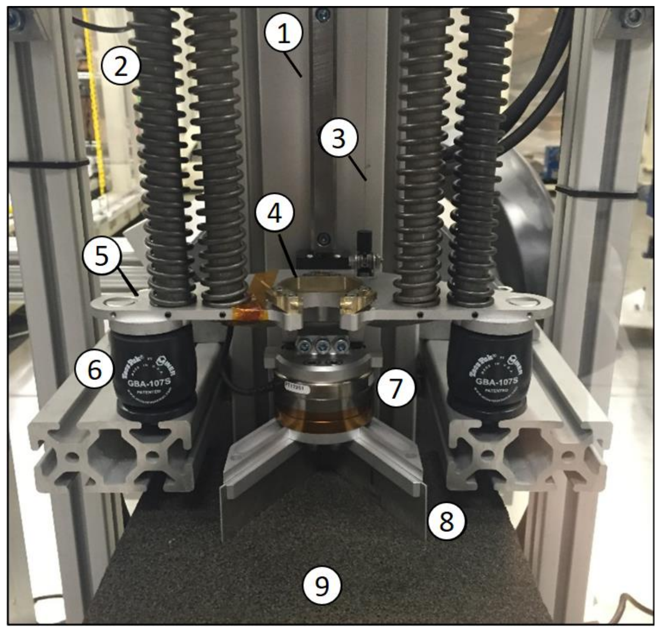

Figure 6. Close up image of Blade Mechanics Penetration Apparatus. Shown are (1) guide rail for central mounting component (2) four energizing springs (of options of 2, 4 or 6), (3) high-speed impact string encoder line, (4) firing release mechanism plate, (5) central mounting component, (6) impact hard stops, (7) 6-d.o.f. force/torque sensor, (8) v-shaped rectangular blade and (9) Grill Brick comet analogue material.

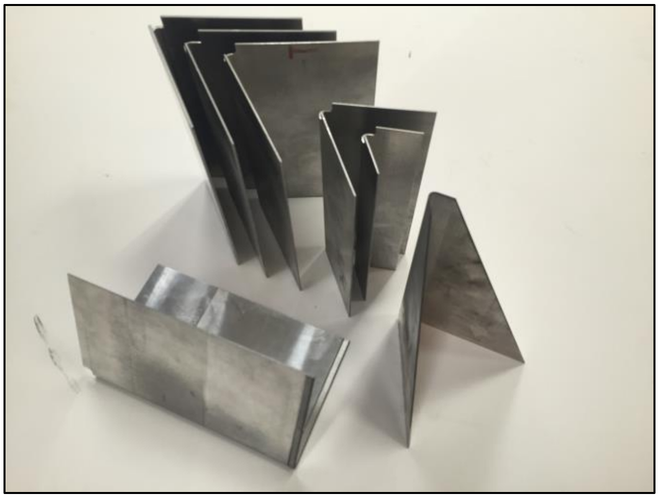

Figure 7. Example of simple test blades used in model parameter determination and model validation. Shown top left: 1mm, 1.5mm and 3mm thickness rectangular blades. Shown middle: half width and 1/3rd width, 1mm thick rectangular blades. Shown bottom right: tapered, 1mm thick blade. Shown bottom left: blade with wider leading tip (2mm tip, 1mm remainder of blade). Not shown: blades with low friction hard coatings (DLC – diamond like carbon). The typical dimensions of full-size unfolded rectangular blade are 184mm width and 150mm height.

The blade test implements and Blade Mechanics Penetration Apparatus were configured to investigate numerous potential effects on penetration resistance due to material and penetrator properties. These include, but are not limited to:

Comet analogue material
- Density/inertial resistance of comet material
- Microstructure strength
- Porousity
- Grain hardness

Blade/penetrator
- Leading edge profile
- Width
- Thickness
- Tapered shape
- Surface hardness
- Velocity of blade
- Penetration depth

Comet Surface Analogue Materials

Two types of materials, Grill Brick and MPACS (the latter developed at NASA JPL [15]), served as comet surface analogues for the blade model development and penetration mechanics investigation. Both are high porousity, low density, brittle materials relevant to comet surface material mechanical property studies and have also been used as analogues in the past.

Grill Brick is a commercially available homogenous material formed of a closed cellular glass structure manufactured by 3M (Figure 8). It was selected for the work described in this paper due to its high repeatability of mechanical properties between material blocks and high homogeneity. This material and similar materials, FOAMGLAS® T4 and F (commercial products), and Foam Glass SRC (utilized by Space Research Centre (SRC) Warsaw) have been used by multiple planetary sampling groups as comet surface analogues for sampling system testing [16] [17] [18].

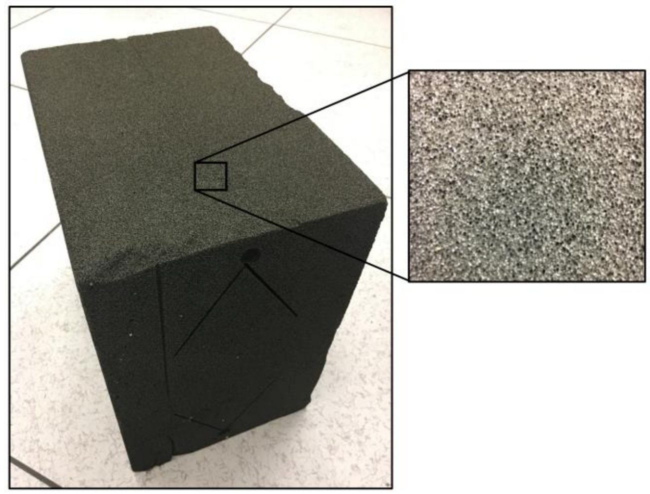

Figure 8. Grill Brick material used as comet surface analogue.

MPACS is a homogeneous geological material that can be produced with weak strengths, brittle failure modes and low densities, while allowing researchers to tune specific mechanical properties [15] (Figure 9). This permits the manufacture of simulants that mimic the mechanical properties expected for a variety of consolidated planetary surfaces.

Figure 9. MPACS comet analogue material. Eight-inch length cube shown.

Although both high porousity, brittle materials, the two have structures that differ significantly. Grill Brick has a structure that consists of unnaturally large pore spaces, very high strength glass bonds and a high bulk compressive strength while MPACS material is formed of a composite structure of bonded grains and induced pore spaces. MPACS was selected as a material for the work described in this paper for its higher fidelity form as a comet surface analogue.

4. EXPERIMENTAL APPARATUS SOFTWARE

Custom MATLAB code with intuitive graphical interfaces was developed to automate experiment data collection and experiment data processing. The software suite was termed Blade Analysis and Modelling (BAM). Data collection software allows easy control of experiment parameters, synchronizes all sensors and actuators, and saves experiment data to an Excel spreadsheet easily understood by humans. Data processing software analyzes experiment results and predicts penetration performance for hypothetical combinations of blades, energizing systems, and penetration materials.

Data Collection

The BAM experiment execution interface (not shown) allows easy access to:

- Set sampling frequency for sensors
- Set sampling duration for recording of experiment (in seconds)
- Select position sensor calibration file
- Select force sensor calibration file
- Tare sensors to set position zero and to ignore static weight of blade system
- Select folder to where experimental results will be saved
- Initiate experiment (requires confirmation on pop-up window for safety)

After user initiates an experiment, the penetrator is launched. Data is temporarily saved for 0.2 seconds before penetrator motion starts, during penetrator motion, and 0.2 seconds after penetrator motion has stopped. The user is then prompted to discard experiment data or automatically save data to an Excel file with columns for time, vertical position, penetration force (in three axes) and torques (in three axes).

Data Processing – Experiment Review and Coefficients

In the BAM data processing Interface (Figure 10) the user can browse to folder containing a BAM-recorded experiment and analyze the results from said experiment. The folder must also contain standardized Excel files describing penetrator parameters, comet surface parameters, and energizing system parameters. The contents of each Excel file will populate their respective panel in the BAM GUI (Figure 10). Additionally, figures will open to help the user judge the quality of the experimental data (Figure 11 and Figure 12).

Model coefficients (Equation 9) in "Comet Surface Parameters" (Figure 10) are estimated from experiment data and do not need to be provided by user. Clicking the radio button next to a coefficient enables and disables the use of the respective term in the model. Therefore, for each coefficient, four values are calculated, one for every model term combination in which that coefficient may be considered. The software will automatically adjust coefficient values depending on which model terms are enabled.

Model Coefficients can also be calculated to simultaneously for multiple experiments. Across these experiments the Penetrator Parameters and Energizing System parameters may vary. Using more experiments and varying parameters across them allows a more reliable calculation of coefficients. Coefficients shown in Table 1 were obtained utilizing this strategy. The coefficients used in the examples shown in the appendix were also obtained through this method.

To judge quality of the model fit to the data, the user can click on "Data and Model" and will be shown Figure 13. For calculation of only penetration resistance, the software uses Equation 9 and the loaded experimental data for position vs. time (top right, Figure 13). For simultaneous prediction of both penetration force and position over time, the software utilizes a dynamic model that considers all significant masses and forces while ignoring all experiment data (bottom right, Figure 13). For energy calculations in Figure 14, the force terms corresponding to the model coefficients activated in the GUI are integrated over distance.

The user can override any parameters in the GUI as needed either to improve the estimate of model coefficients or to explore the predicted effect on penetration performance. The original value for all parameters is shown as "default" next to the respective entry box. The user may reset all boxes to default by clicking "Reset".

Data Processing – Analysis of Penetration Performance

In the "Analysis Setup" panel of Figure 10 the user can select any two parameters to study their effect on the energy required for penetration (Figure 14 and Figure 15). For each parameter, positive and negative deltas are set to determine the range of values to be explored. A general resolution to determine the number of points within that range is then set.

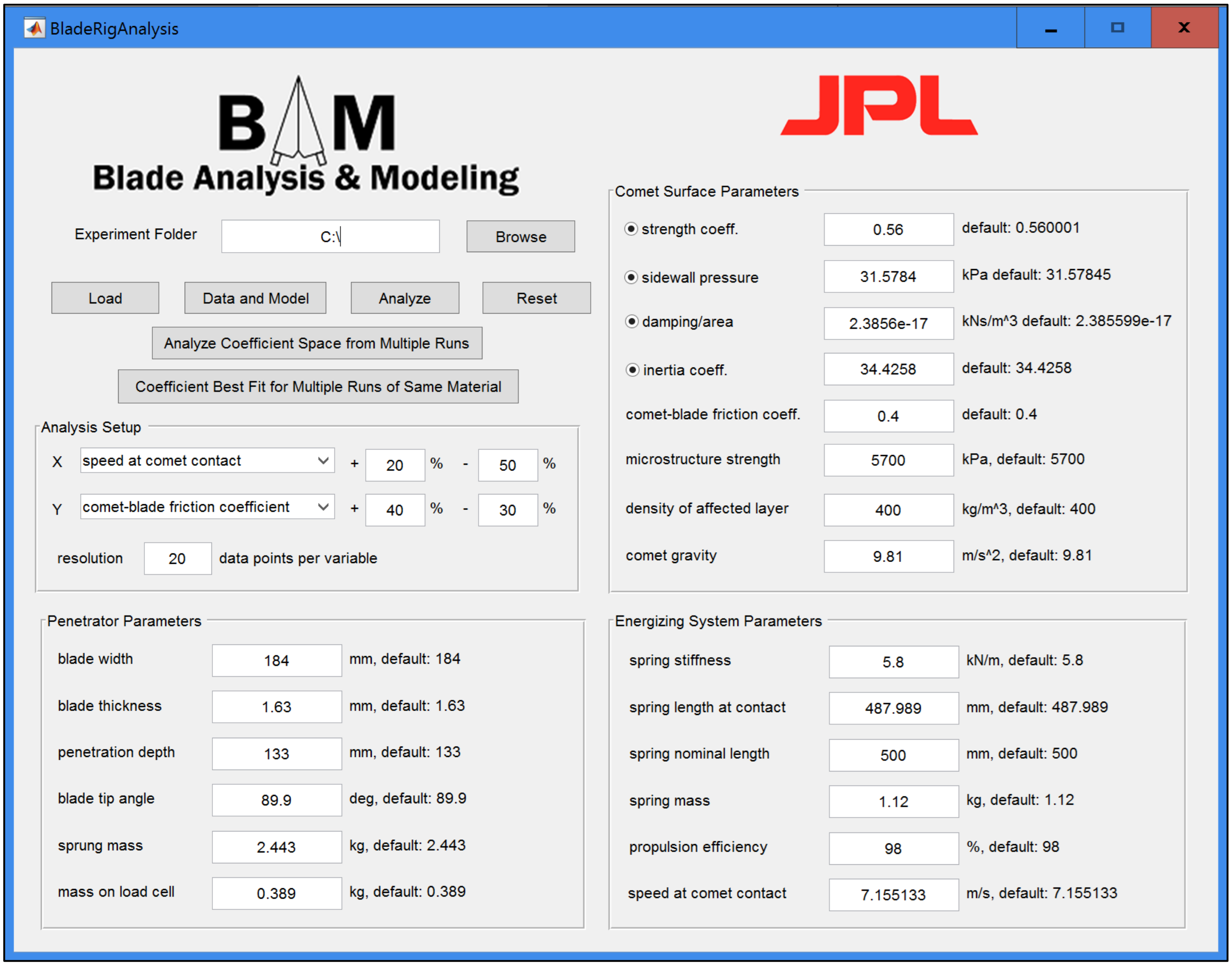

Figure 10. BAM Analysis GUI. User can study physical experiments and perform theoretical experiments.

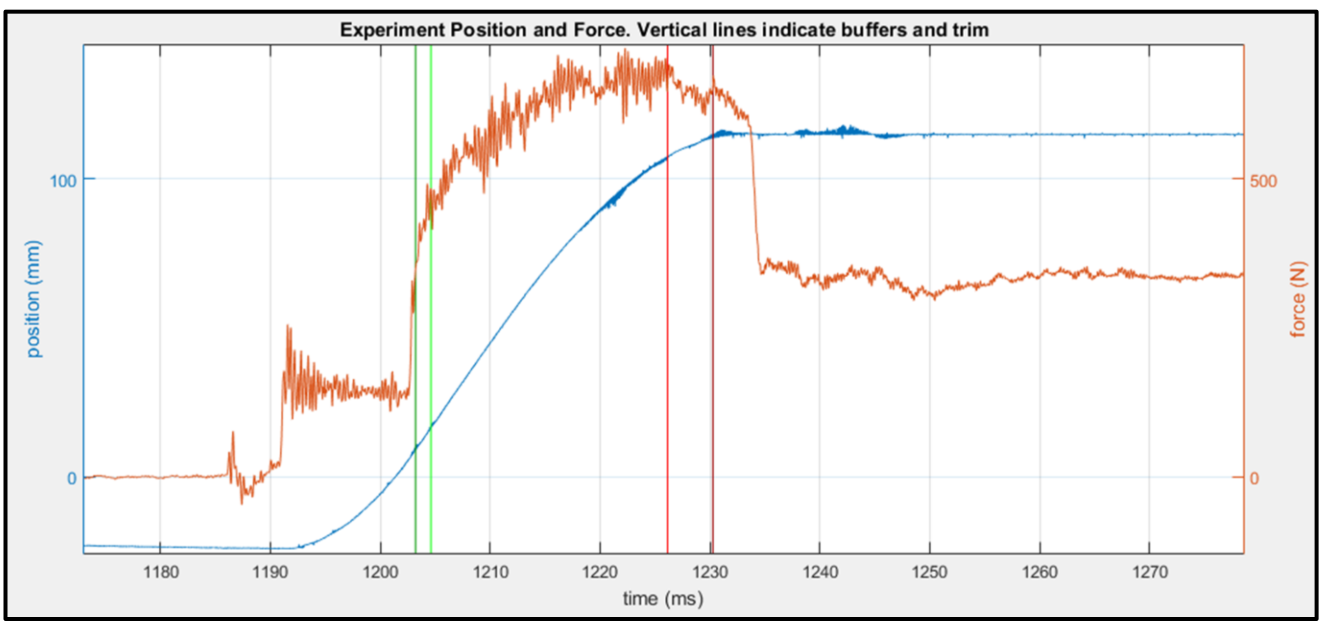

Figure 11. Sample raw data from experiment. Outermost colored vertical lines are limits of stored data. Innermost colored vertical lines are limits of analyzed data. Full penetration was not achieved and springs are still applying downward force at end of experiments. Inertial force from blade mass can be observed at experiment start.

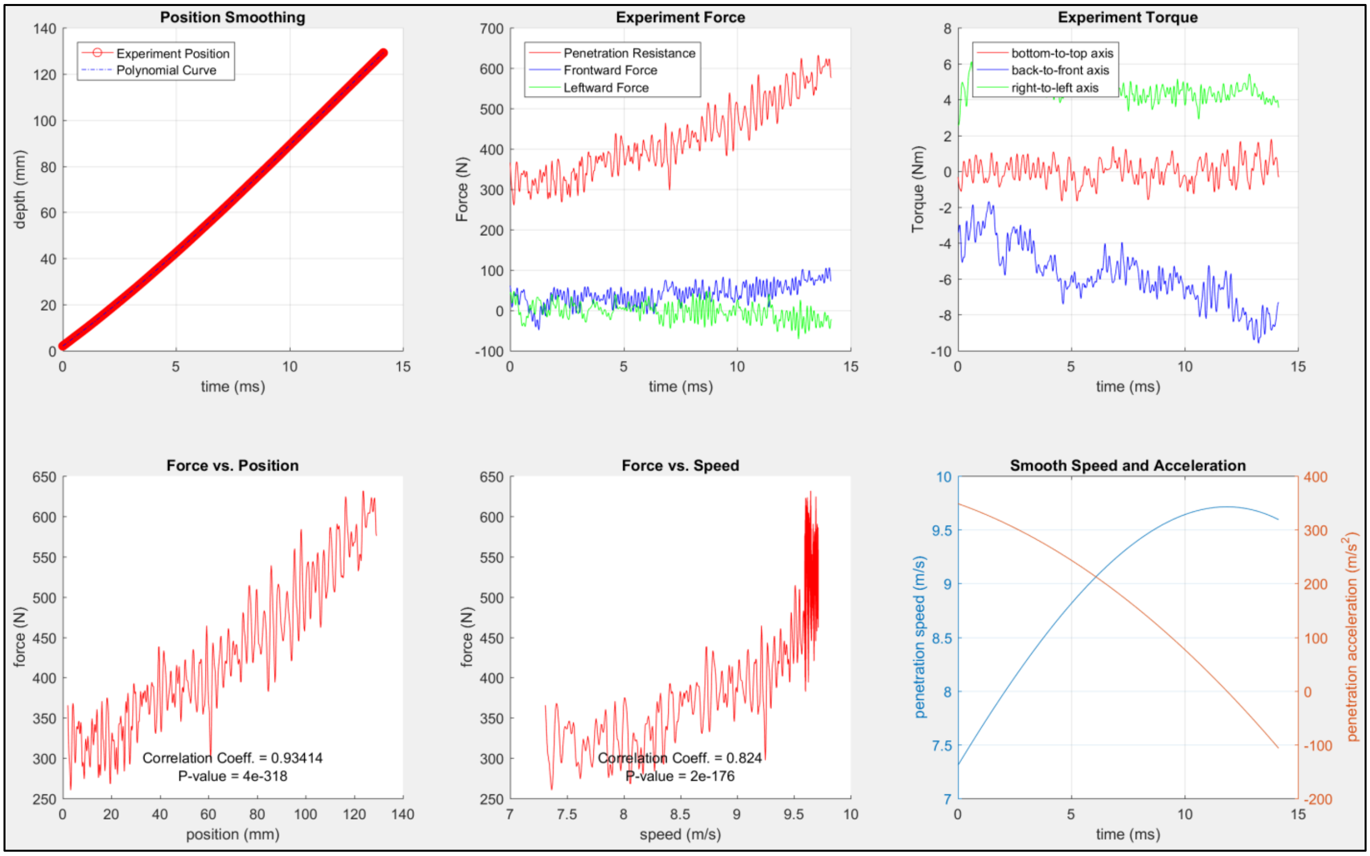

Figure 12. Visualization of experiment measurements upon file loading: position, force/torques, speed, acceleration.

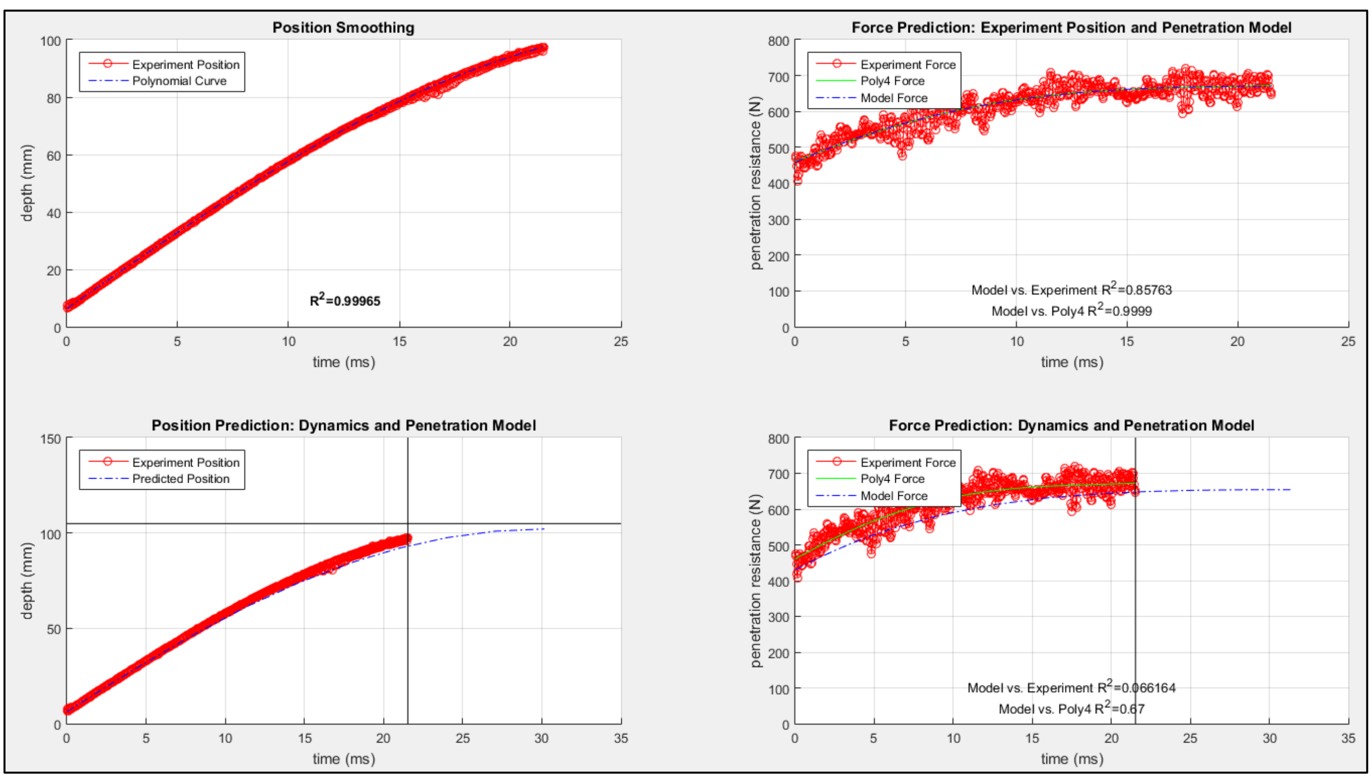

Figure 13. Capability to compare dynamic/penetration model results to actual forces and motion.

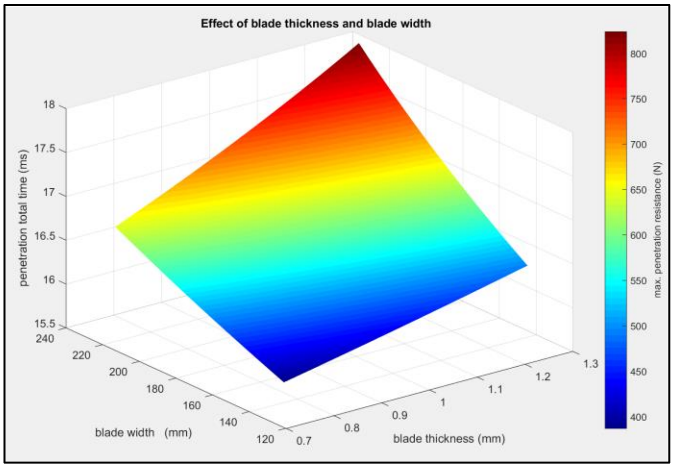

Figure 14. Example of using surface plot to assess the effect of blade width and blade thickness on penetration time and maximum penetration resistance.

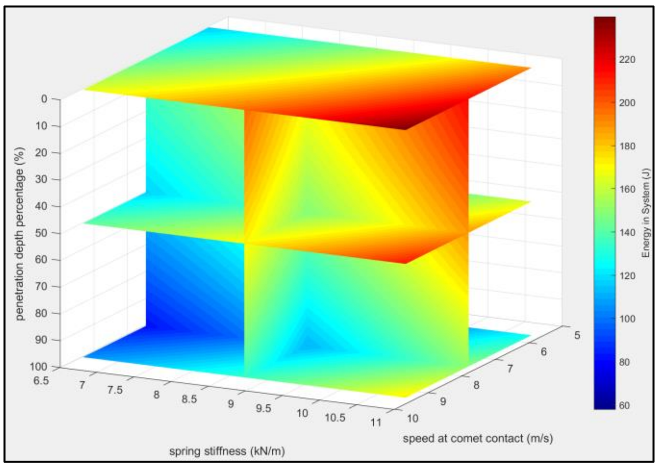

Figure 15. Example 4-D plot to assess effect of varying penetrator or comet analogue material parameters. Color shows residual kinetic energy at penetration depth.

5. Experimental Results and Validation

The proposed high-speed blade penetration mechanics model introduced in Section 2 was exercised over a range of penetrator parameters, energizing system parameters and materials. This section will explain the validation results of the model and will primarily focus on the Grill Brick material since it offers higher repeatability of results due to little variation in mechanical properties. The model coefficients and parameters of MPACS are shared to illustrate the difference between to material types.

An initial set of twelve blade penetration tests were conducted for each material to determine the four model coefficients. For Grill Brick, MPACS B, and MPCS C coefficients were optimized simultaneously for multiple experiments. That is, coefficients that minimized the net error across all experiments were selected. For Grill Brick, MPACS B and MPACS C, the damping coefficient was enabled as a degree of freedom but was calculated as approximately zero. For MPACS D coefficients were optimized for a single experiment. In estimation of coefficients for a single experiment, to reduce the model degrees of freedom and increase stability, the viscous damping coefficient is recommended be set to zero (which was done).

The best coefficients estimates are shown in Table 1 along with known materials properties of the comet surface analogues.

Table 1. Material Coefficients

	Measured Material Parameters Used in Model		
Material	Density [g/cc]	Microstructure Strength [kPa]	Blade (6061AL) Friction Coefficient
Grill Brick	0.11	1630	0.75
MPACS B	0.29	2000	0.4
MPACS C	0.40	6000	0.4
MPACS D	0.68	40000	0.4

	Model Coefficients from Experiments (BAM) (See Equation 9)			
Material	S correction factor	P [kPa]	C	K
Grill Brick	1.6	7.07	0	46
MPACS B	0.6	12.5	0	10
MPACS C	0.6	31.6	0	34.4
MPACS D	0.25*	530*	0*	70*

*: estimated from single experiment

	Other Mechanical Properties for Reference	
Material	Cone Penetration Resistance [MPa]	Unconfined compressive strength [kPa]
Grill Brick	0.5-0.75	1000
MPACS B	0.75-2.0	100-125
MPACS C	5.0-8.0	200-250
MPACS D	20-25	700-850

For all subsequent modeling - for modeling verification purposes - and for penetrator performance studies, the values in Table 1 were used with good success. Examples results for predicting the response of a blade penetrator are shown in the Appendix B. The dynamic response of the high-speed blade to penetration resistance is well captured in the force-time space as well as force-position space.

Other simpler methods to predict penetration resistance can be applied but do not yield the results needed to represent the dynamic aspects of a penetrator at 0m/s to 15m/s. A comparison of the results of these other methods is shown in Figure 16. The Cone Penetration Test (CPT) is based laboratory tests utilizing a standard cone penetrometer. Unconfined Compressive Strength (UCS) utilizes the compressive strength of the material and the penetrator area.

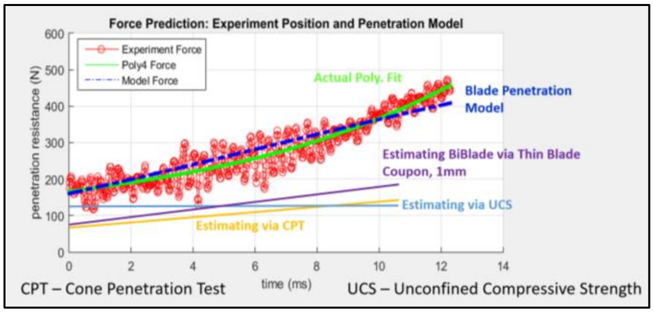

Figure 16. Comparison of penetration resistance model developed to other methods of estimating net resistance in Grill Brick.

Study on reduction of energy lost to friction

Friction is a major source of penetration resistance in the materials tested and, as such, an area of opportunity for improving a penetrator's performance (Figure 17). Two strategies were selected for reducing penetration resistance:

A) Improve blade surface hardness to reduce friction coefficient.

B) Make blade leading edge wider than blade body, thus preventing the blade sidewalls from experiencing significant normal force from contacting the penetration cavity walls.

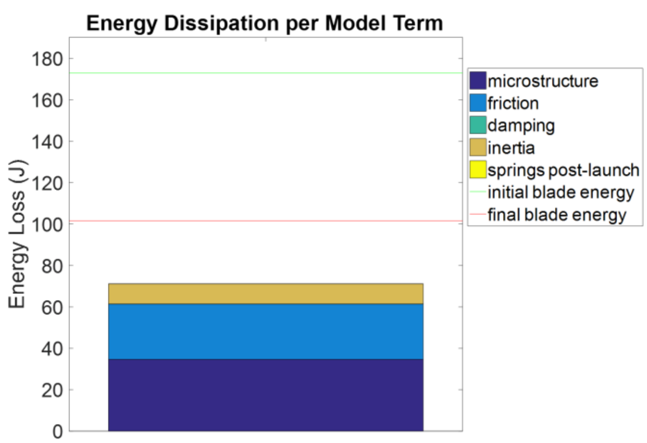

Figure 17. Friction is a significant source of penetration resistance for thin-blade penetrators in the materials tested. It should be noted that inertial and microstructural forces have been reduced by the blade's thin frontal profile when compared to thicker penetrators.

It was found that reducing the friction coefficient has benefits for peak penetration force and penetration time with no significant trade-offs. On the other hand, while making the tip thicker than the body does decouple the penetration resistance from depth, it also generates a higher penetration resistance throughout. Figure 18 displays results implementing the two strategies compared to a nominal 1mm blade to reduce resistance attributed to sidewall friction.

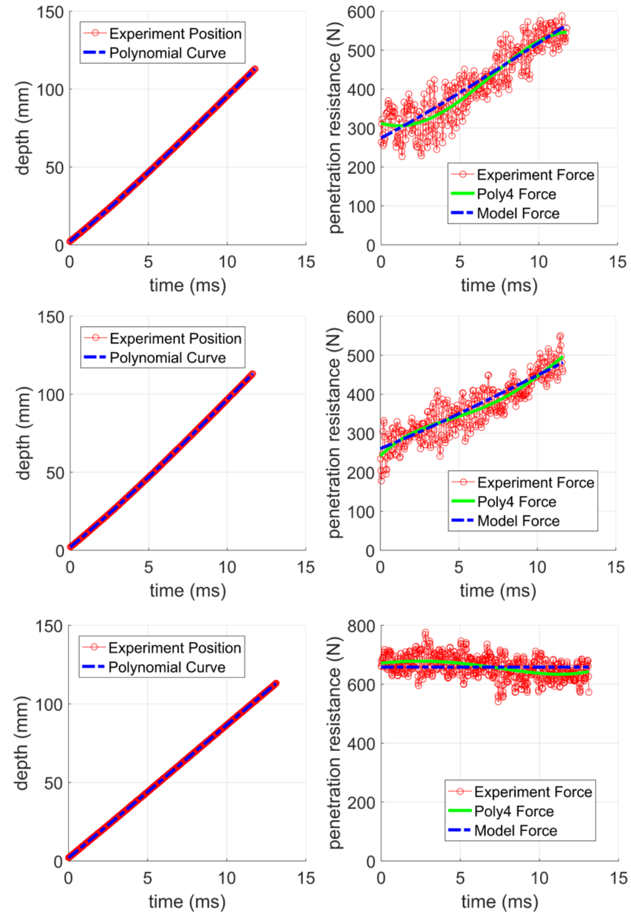

Figure 18. Examples of results from strategies to reduce friction force during penetration. Top row: 6061 Al 1mm thick blade, middle row: Ti-6Al-4V with low friction hard coating (DLC, "diamond-like carbon" coating) 1mm thick blade (Strategy A), bottom row: 6061 Al blade with leading edge 2mm thick but rest of blade body only 1mm thick (Strategy B).

6. IMPORTANT FINDINGS RELATED TO DESIGN OF PENETRATORS

The investigation of energy dissipated for each model term yields important results when considering design of high-speed blade penetrators (5m/s to 15m/s) into comet surface-like materials. The quasi-static strength of the material (microstructure strength, compressive strength and even cone penetration resistance) only plays a partial role in the total penetration resistance on a high-speed blade. Friction against the blade sidewall and inertial resistance of the comet material, combined, dissipate similar or more energy as the material strength. The inertial resistance term is a combination of blade impact velocity (second order), blade frontal area and comet material density. Reducing impact velocity by increasing penetrator mass can reduce the energy loss via inertial resistance (comet density). Even for low density material, rapid acceleration to tens of meters per second requires forces exceeding that of the typical microstructure strength of materials of interest. Efforts to reduce sidewall friction can also significantly decrease penetration resistance. As suggested by the friction term, both sidewall pressure and friction coefficient can be exploited to reduce resistance. A wider leading edge of the blade (Figure 7) can create a gap or reduce pressure by allowing space for crushed materials to flow into. Coatings to reduce the coefficient of friction between the blade parent material and penetrated material can be highly beneficial.

7. CONCLUSION

A comet surface penetration model useful for predicting penetration performance and improving the design of penetrators is presented. The model can also be used to estimate the mechanical properties of comet analogues from multiple experiments.

The model was demonstrated for material types in the family of porous, brittle, crushable structure generally accepted as a representation of comet nuclei surface materials.

Model and created software high impact benefits are:

- Inform/optimize design parameters effects on blade penetration resistance via parametric form of model
- Energy dissipation evaluation for each model term in model prediction or physical test
- Analytical model can be easily integrated into full system (i.e. spacecraft level) simulation such as multi-body dynamics package
    - blade reaction forces a function of position and speed.
- Informs material properties on sampling ability
    - use to identify simulates (reduce # or envelope corners w.r.t. blade-material mechanics)
- Map materials to penetration performance continuum instead of simple experimental pass/fail (i.e. can interrogate performance with respect to resistance mechanics such as friction, microstructure stretch, inertial resistance, etc.)
- Predict maximum material strength penetrable given spring input (or any other type of input/limit)

APPENDICES

A. VALIDATION TESTS GRILL BRICK

Appendix A has 6 randomly selected tests from a pool of 58 runs in Grill Brick material (constant material properties) while four different penetrator parameters are varied. These parameters are spring energy, blade thickness, blade width and accelerated mass (effects velocity). The actual force versus time is shown in red (polynomial fit in green). The model predicted force versus time is shown in blue. Note that model coefficients are preselected and constant across all tests while know penetrator parameters are inputted (i.e mass, geometry, energy, etc). Pre-determined coefficients are $C_{\mu\text{-struct.}}$=1.6, $C_{friction}$ = 7.07kPa $C_{visc.\ damp.}$ =0, $C_{inertia}$ =46. Known properties are Micro-structure strength = 1630kPa, density = 0.11g/cc, coefficient of friction between blade-material = 0.75. Good agreement of model predicts versus actuals is shown.

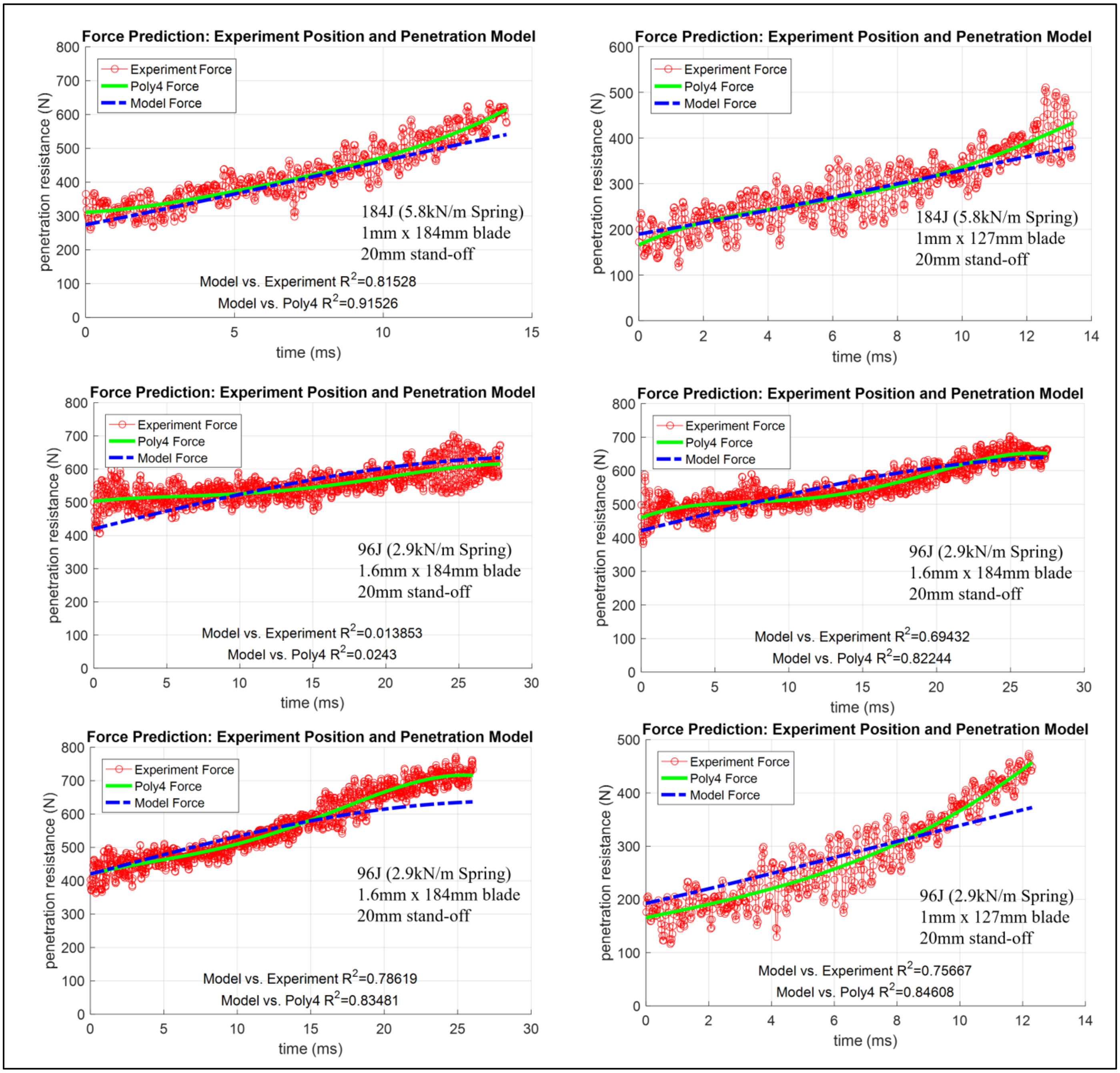

B. Validation Tests 2 of 2, MPACS C

Appendix B has 6 randomly selected tests for MPACS C while blade thickness is varied. The actual force versus time is shown in red (polynomial fit in green). The model predicted force versus time is shown in blue. Note that model coefficients are preselected and constant across all tests while know penetrator parameters are inputted (i.e mass, geometry, energy, etc). Pre-determined coefficients are $C_{\mu\text{-struct.}}$=0.6, $C_{friction}$ = 31.6kPa $C_{visc.\ damp.}$ =0, $C_{inertia}$ =34.4. Assumed properties are Micro-structure strength = 5600 - 8200kPa (measured for each block), density = 0.4g/cc, coefficient of friction between blade-material = 0.4. Good agreement of model predicts versus actuals is shown.

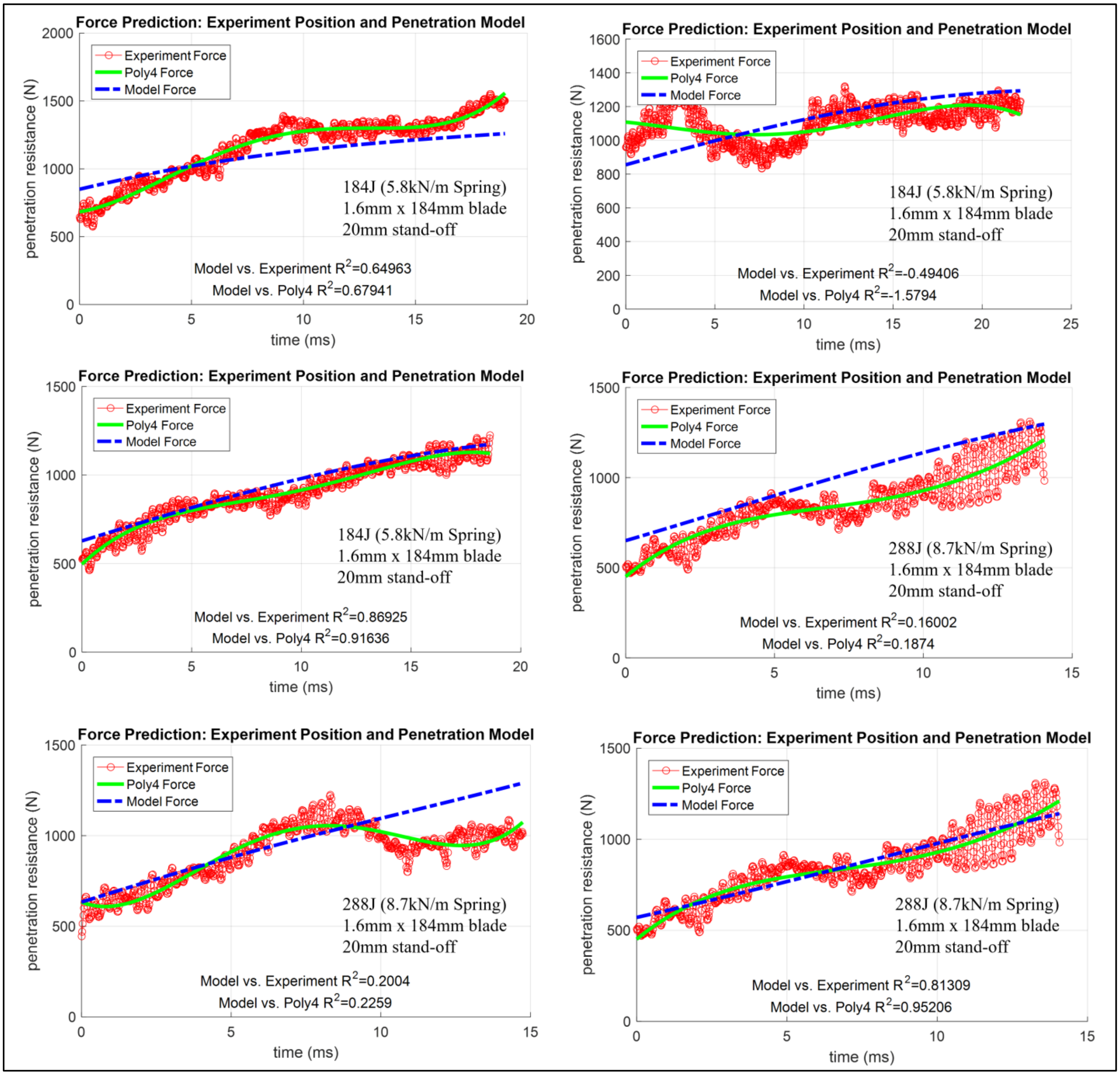

C. Sensitivity Analysis for Simulated Penetration

Appendix C shows the effect of adjusting penetrator design variables. The default configuration is: blade width = 15cm, blade thickness = 1.5mm, blade leading edge angle = 45°, spring mass = 1kg, spring stiffness = 10kN/m, spring nominal length = 50cm, spring compressed length = 30cm, surface offset (initial distance from blade tip to comet surface) = 15cm, penetration depth = 13cm. The simulant properties are shown in Section 5. Empty values did not achieve full penetration.

Energy lost to penetration resistance

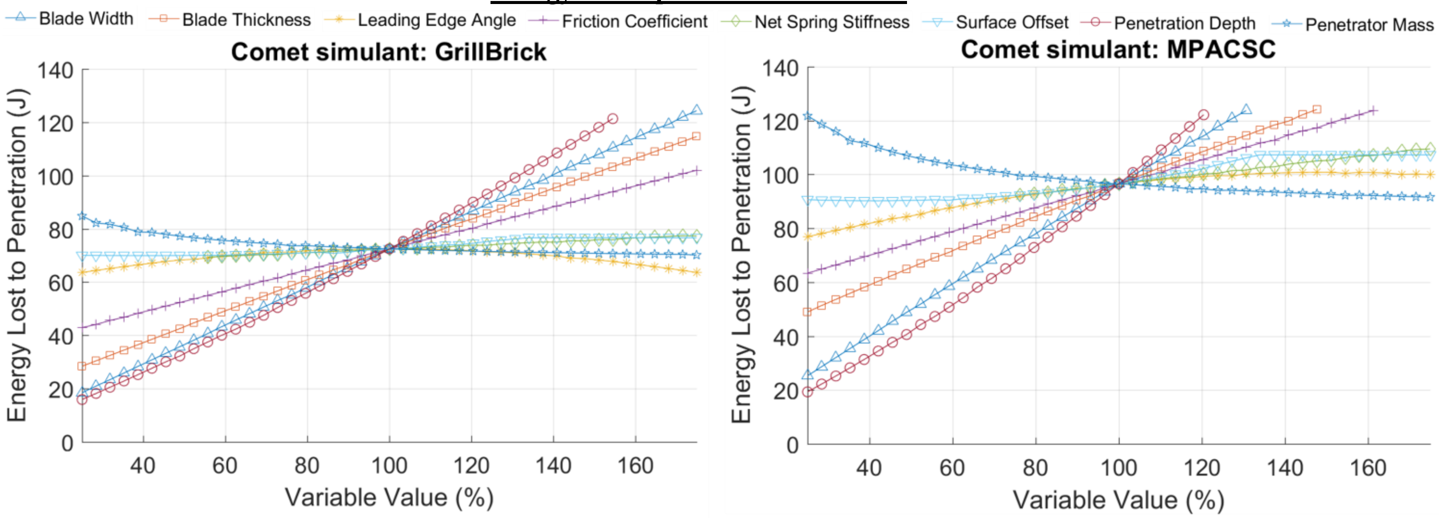

Maximum penetration resistance

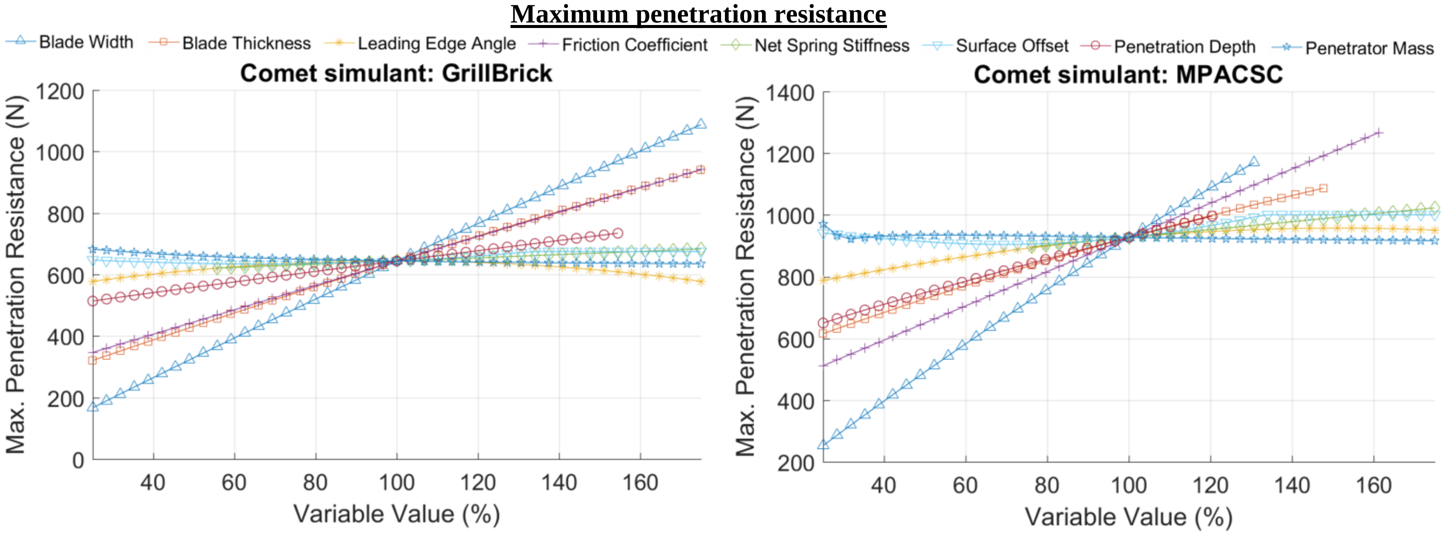

Time to achieve complete penetration

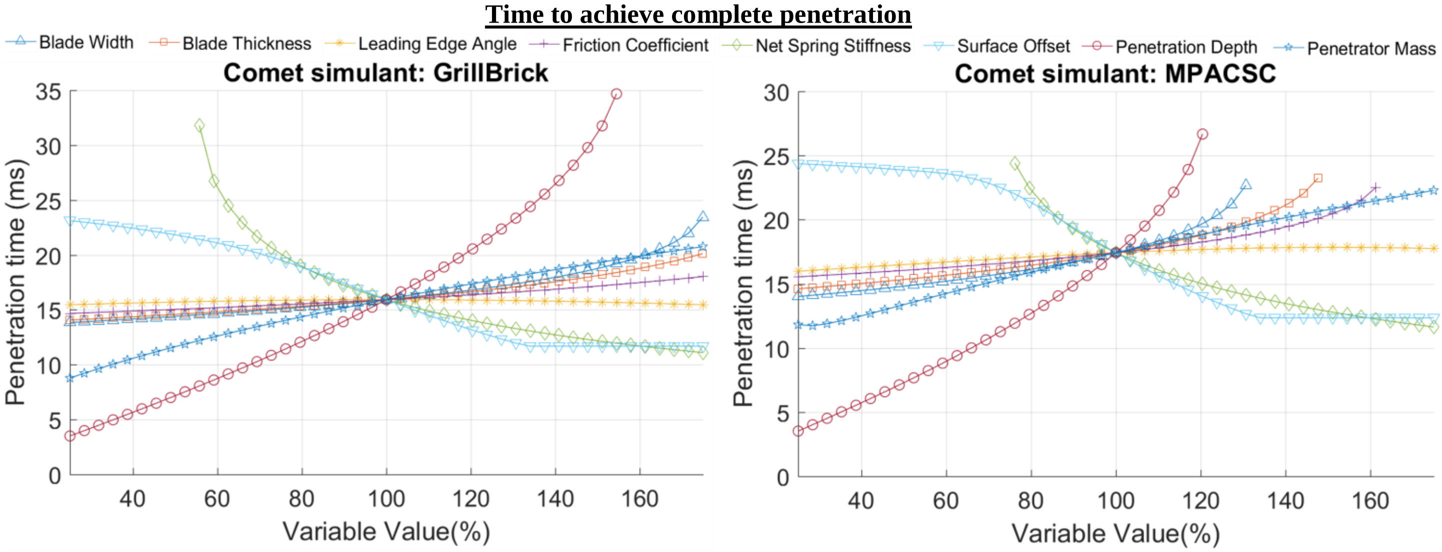

Disclaimer: Reference herein to any specific commercial product, process, or service by trade name, trademark, manufacturer, or otherwise, does not constitute or imply its endorsement by the United States Government or the Jet Propulsion Laboratory, California Institute of Technology.

ACKNOWLEDGEMENTS

The research described in this publication was carried out at the Jet Propulsion Laboratory, California Institute of Technology, under a contract with the National Aeronautics and Space Administration (NASA).

REFERENCES

[1] M. F. A'Hearn, M. S. Belton, W. Delamere, J. Kissel, K. Klaasen, L. McFadden, K. Meech, H. Melosh, P. Schultz, J. Sunshine, P. Thomas, J. Veverka, D. Yeomans, M. W. Baca, I. Busko, C. Crockett, S. M. Collins, M. Desnoyer and e. al., "Deep Impact: Excavating Comet Tempel 1," *Science*, vol. 310, no. 5746, pp. 258-264, 2005.

[2] J. Biele, S. Ulamec, M. Maibaum, R. Roll, L. Witte, E. Jurado, P. Muñoz, W. Arnold, H.-U. Auster, C. Casas, C. Faber, C. Fantinati, F. Finke, H.-H. Fischer, K. Geurts, C. Güttler and e. al., "The landing(s) of Philae and inferences about comet surface mechanical properties," *Science*, vol. 349, no. Philae's first days on the comet, 2015.

[3] N. I. Kömle, A. J. Ball, G. Kargl, T. Keller, W. Macher, M. Thiel, J. Stöcker and C. Rohe, "Impact penetrometry on a comet nucleus - interpretation of laboratory data using penetration models," *Planetary and Space Science*, vol. 49, no. 6, pp. 575-598, 2001.

[4] P. Backes, C. McQuin, M. Badescu, A. Ganino, H. Manohara, Y. Bae, R. Toda, N. Wiltsie, S. Moreland, J. Grimes-York, P. Walkemeyer, E. Kulczycki, C. Dandio, R. Smith, M. Williamson and e. al, "Sampling System Concepts for a Touch-and-Go Architecture Comet Surface Sample Return Mission," in *AIAA SPACE Conference and Exposition*, San Diego, CA, 2014.

[5] A. ElShafie and E. Heggy, "How hard is the surface of comet nucleus? A case study for comet 67P/Churyumov-Gerasimenko," in *46th Lunar and Planetary Science Conference*, Houston, TX, 2015.

[6] J. Biele, S. Ulamec, L. Richter, J. Knollenberg, E. Kührt and D. Möhlmann, "The putative mechanical strength of comet surface material applied to landing on a comet," *Acta Astronautica*, vol. 65, pp. 1168-1178, 2009.

[7] S. Colbeck, "The kinetic friction of snow," *Journal of Glaciology*, vol. 34, no. 116, 1988.

[8] J. B. Johnson and M. Schneebeli, "Characterizing the microstructural and micromechanical properties of snow," *Cold Regions Science and Technology*, pp. 91-100, 1999.

[9] G. K. Swinzow, "Terminal Ballistics in Ordinary Snow - Small Arms Fire Attenuation," CRREL Technical Report - 238, Hanover, NH, 1972.

[10] H.-P. Marshall and J. B. Johnson, "Accurate inversion of high-resolution snow penetrometer signals for microstructural and micromechanical properties," *Geophysical Research*, vol. 114, 2009.

[11] H. O. K. Kirchner, G. Michot, H. Narita and T. Suzuki, "Snow as a foam of ice: plasticity, fracture and the brittle-to-ductile transition," *Philosophical Magazine*, vol. 81, no. 9, pp. 2161-2181, 2001.

[12] L. Gibson and M. Ashby, Cellular Solids: Structures and Properties, Cambridge University Press, 2001.

[13] C. Borstad and D. McClung, "Thin-blade penetration resistance and snow strength," *Journal of Glaciology*, vol. 57, no. 202, 2011.

[14] V. Alí-Lagoa, M. Delbo and G. Libourel, "Rapid Temperature Changes and The Early Activity on Comet 67P/Churyumov-Gerasimenko," *The Astrophysical Journal Letters*, vol. 810, 2015.

[15] E. M. Carey, G. H. Peters, L. Chu, Y. M. Zhou, B. Cohen, L. Panossian, M. Choukroun, J. R. Green, P. Backes, S. Moreland and L. Shiraishi, "Development and characteristics of mechanical porous

ambient comet simulants (MPACS) as comet surface analogs," in *47th Lunar and Planetary Science Conference*, The Woodlands, Texas, 2016.

[16] M. Paton, S. Green, A. Ball, J. Zarnecki and A. Harri, "Using inertia of spacecraft udring landing to penetrate regoliths of the solar system," *Advances in Space Research*, vol. 56, no. 6, pp. 1242-1263, 2015.

[17] T. Spohn, J. Knollenberg, A. Ball, M. Banaszkiewicz, J. Benkhoff, M. Grott, G. Grygorczuk, C. Hüttig, A. Hagermann, G. Kargl, E. Kaufmann, N. Kömle, E. Kührt, K. Kossacki, W. Marczewski, I. Pelivan, R. Schrödter and K. Seiferlin, "Thermal and mechanical properties of the near-surface layers of comet 67P/Churyumov-Gerasimenko," *Science*, vol. 349, no. 6247, 2015.

[18] K. Zacny, P. Chu, J. Spring, S. Ford and G. Paulsen, "Pyramid Comet Sampler (PyCoS)," in *AIAA SPACE 2015 Conference and Exposition*, Pasadena, CA, 2015.

[19] P. C. Thomas, J. Veverka, M. J. Belton, A. Hidy, M. F. A'Hearn, T. Farnham, O. Groussin, J.-Y. Li, L. A. McFadden, J. Sunshine, D. Wellnitz, C. Lisse, P. Schultz, K. J. Meech and W. A. Delamere, "The shape, topography, and geology of Tempel 1 from Deep Impact observations," *Icarus*, vol. 191, pp. 51-62, 2007.

BIOGRAPHY

Scott Moreland *received his B.S. degree from University of Toronto and his M.S. and Ph.D. degrees in Mechanical Engineering from Carnegie Mellon University. He joined JPL in the fall of 2013 as a member of the Robotic Vehicles and Manipulators Group. His work typically involves systems that interact with the ground either for mobility or sampling purposes. Of particular interest to Dr. Moreland is the development of traction devices for extreme surface materials and micro-gravity environments. His experience includes the design and fielding of robotic vehicles, mechanism/machine design and mechanical systems testing.*

Guillermo F. Díaz Lankenau *received a B.S. in Mechatronics Engineering from Tec de Monterrey in 2012. After graduation, he worked as an Engineer at John Deere until joining Massachusetts Institute of Technology (MIT) in 2014 to pursue a graduate science degree in Mechanical Engineering. At MIT Guillermo is a researcher at the Global Engineering and Research Laboratory (GEAR Lab) where he is developing a mechanized replacement for animal power in Indian farms. During his studies Guillermo has interned at Mercedes Benz, NASA Goddard Space Flight Center, Carnegie Mellon Robotics Institute, and NASA Jet Propulsion Laboratory. Guillermo's engineering experiences have mostly revolved around robotics, soil-machine interactions, and product design.*

Isabel Naranjo De Candido *is currently a Master's degree student in Nuclear Engineering at University of Pisa. She received a Bachelor's degree in Mechanical Engineering in 2015 at the University of Pisa as well. Isabel is also an Allieva Ordinaria at Scuola Superiore Sant'Anna. In 2011, Isabel participated to "Zero Robotics High School Tournament" (MIT, NASA, ESA), in October 2013 spent one month at Chongqing University (China) as an exchange student, in 2015 interned at the Jet Propulsion Laboratory (USA) and finally in September, October 2016 interned at the Fermilab (USA).*

Mircea Badescu *is a Technologist at the NDEAA lab of the Jet Propulsion Laboratory. He joined JPL in February 2005 after serving as a Caltech Postdoctoral Scholar for a year. He received the Ph.D. degree in robotics in mechanical and aerospace engineering, from Rutgers University, in 2003. Prior to graduate school he worked for the Romanian Navy on the design of underwater diving equipment. He has experience on design integration of power ultrasonic piezoelectric devices, planetary and low gravity sampling systems, extreme environments devices, instruments for planetary exploration, optical components for telescopes, and optimal design of self-reconfigurable robots using parallel platforms as modules. He has experience in organizing and conducting field tests including glaciers, Antarctica, and desert. He has expertise on designing haptic devices for vehicular instruments control and automotive smart clutches. He is coauthor of 91 publications, 11 patents, 57 NTRs, and recipient of 39 NASA awards.*

Paul Backes (Member, IEEE) *is the Group Supervisor of the Robotic Manipulation and Sampling group at Jet Propulsion Laboratory, California Institute of Technology, where he has been since 1987. He received the BSME degree from U.C. Berkeley in 1982, MSME degree from Purdue University in 1984, and Ph.D. in Mechanical Engineering from Purdue University in 1987. Dr. Backes received the 1993 NASA Exceptional Engineering Achievement Medal for his contributions to space telerobotics, 1998 JPL Award for Excellence, 1998 NASA Software of the Year Award Sole Runner-up, 2004 NASA Software of the Year Award, and 2008 IEEE Robotics and Automation Award. He has served as an Associate Editor of the IEEE Robotics and Automation Society Magazine.*